Magnetic imaging of spin waves and magnetic phase transitions with nitrogen-vacancy centers in diamond

Bertelli, I.

6

SENSING CHIRAL MAGNETIC NOISE VIA QUANTUM IMPURITY RELAXOMETRY

Via the fluctuation-dissipation theorem, the magnetic fluctuations of a system are related to its susceptibility, which provides information about the system's excitations. Thermally-excited spin waves are a source of such fluctuating magnetic fields, which can be locally probed by the electron spin of single NV centers in diamond. Focusing on a nickel thin film, we study the magnetic-noise spectrum of thermally-excited spin waves via relaxometry measurements. We further analyze the distance- and field-dependence of the magnetic fluctuations, finding a good agreement with a theoretical model based on the chiral coupling between the spin-wave stray fields and the NV transitions. We detect discrepancies at the ferromagnetic resonance frequency of nickel, which we address by performing additional measurements of coherent spin waves, suggesting the presence of spatial field inhomogeneities.

Parts of this chapter have been published in *Physical Review B* **102**, 220403 (2020) by A. Rustagi, **I. Bertelli**, T. van der Sar, P. Upadhyaya. Helena La provided the code for the magnetic noise calculations.

6.1. INTRODUCTION

Magnetic noise can be the result of charge[1, 2] and spin[3, 4] fluctuations. Via the fluctuation-dissipation theorem, such noise can be related to the intrinsic properties and excitations of a system[5], which are reflected in the conductivity and susceptibility tensors. Because of their non-invasive and point-like nature, single NV electron spins in diamond are well suited to probe such fluctuations locally and quantitatively via NV relaxometry. Therefore, single-NV relaxometry has been proposed as a tool to probe the normal metal-superconductor transition[6, 7], the antiferromagnet(AFM)-ferromagnet metamagnetic phase transition[8], the AFM chemical potential[9], AFM domain walls[10], the electron-phonon instability in graphene [11], the emergence of exotic quantum spin-liquid phases with topological character[4], magnetic monopoles in spin ice[12], one-dimensional edge states [13] and magnon sound modes in magnets in the hydrodynamic regime[14].

In a magnet, quantifying the magnetic field noise can grant access to the spin chemical potential[15], which indicates the tendency of spins to diffuse, or to the power spectral density of the magnetic field, which reflects the system's excitations[16, 17, 22]. It has been predicted that quantifying the distance dependence of magnetic noise in the spin-wave gap of a magnet is an effective tool in detecting a transition between the diffusive and ballistic-like transport of spin waves[3, 23]. The crossover between the different transport regimes should take place at a distance similar to the spin diffusion length[3].

Here, we investigate thermal spin waves by characterizing the relaxation rate of single NV centers at a distance of $\sim 0-300$ nm from a nickel thin film. We analyze these results according to the theoretical model describing the chiral coupling of the spin-wave fields with the NV transitions, developed in Chapter 3. We find a remarkable agreement between the measured distance- and field-dependence of the NV relaxation rates with the theoretical model. In particular, the model accurately predicts the amplitude of the magnetic-field noise without free parameters. We also detect the unexpected presence of a large noise at frequencies below the ferromagnetic resonance (FMR) of nickel, where the noise should be suppressed. We perform additional measurements of NV Rabi oscillations to probe coherent spin waves. Close to the FMR, we observe that the Rabi frequencies of NV centers in nickel-covered areas are strongly modified by the spin-wave modes in the magnetic film. This indicates that driving the system with a microwave field excites spin waves whose stray fields add to the direct drive field. The local variations between NV centers suggest the presence of inhomogeneities of the magnetic surface and granularity of the spacer layer, possibly causing large local stray fields variations.

6.2. RESULTS

SYSTEM GEOMETRY

To have access to isolated NV defects at different distances from a magnetic film, we fabricate a SiO_2 spacer layer of increasing thickness on a diamond with shallow single-NV centers, on top of which we grow a 40 nm-thick layer of nickel (Fig. 6.1a). Individual NV

spins are addressed from below, using a confocal microscope (Section 2.1.3), both in the bare diamond and under the nickel layer (Fig. 6.1b). All the NV defects investigated in this chapter possess the same crystallographic orientation.

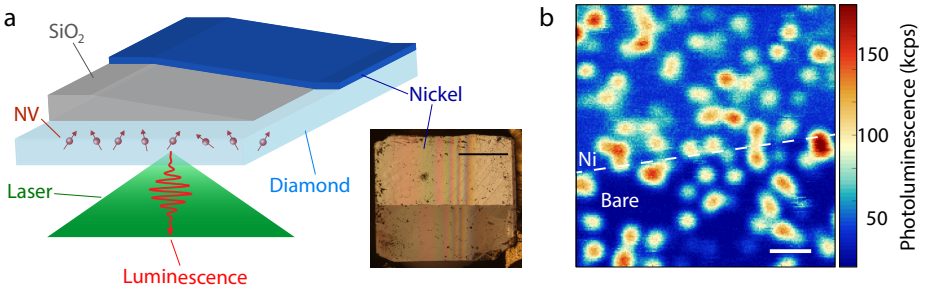

Figure 6.1: System geometry. (**a**) A SiO_2 spacer layer of varying thickness (0-1 μm) is grown on top of a diamond containing NV centers that can be individually addressed using a confocal microscope. A 40 nm-thick nickel layer is evaporated onto half of the diamond-spacer substrate. Inset: optical micrograph of the sample. The top half of the diamond is coated with nickel. The spacer layer thickness changes horizontally, as can be deduced from the optical interference fringes resulting from the commensurability of the light wavelength and the spacer thickness. Scale bar: 500 μm. (**b**) Photoluminescence image of the sample, showing (mostly) single NV centers as bright spots of ~120 thousands counts per second. Much brighter areas indicate the presence of more than one NV per diffraction-limited spot. The background signal is higher where the diamond is coated with the nickel film (top half). Scale bar: 1 μm.

CHARACTERIZING THE EXCITATIONS OF THE SYSTEM

We start characterizing the system by performing electron spin resonance (ESR) measurements (Section 2.2.2), at increasing values of the static field oriented along the NV center axis, at a location where the SiO_2 is absent (Fig. 6.2a). When the ω_- frequency is close to the FMR (bottom of the spin-wave band), the $|0\rangle \leftrightarrow |-1\rangle$ transition shows an increased contrast and width compared to $|0\rangle \leftrightarrow |+1\rangle$. This indicates an efficient driving of the NV spins by the stray fields of spin waves with frequencies close to the FMR. An increased contrast is consistent with the larger driving field (Section 2.2.2.2), and an increased width is consistent with a lifetime reduction caused by magnetic noise (Section 3.5). Surprisingly, at the exact field-and-frequency where the calculated FMR of the nickel film crosses the ω_- ESR transition, we notice a clear and abrupt reduction of the contrast and width of the ESR dip (Fig. 6.2b). At this moment, we do not know the cause of such changes.

DETECTING MAGNETIC NOISE BY NV RELAXOMETRY

The magnetic-noise spectrum of a system provides information regarding its excitations. We probe the magnetic fluctuations of thermal spin waves via NV relaxometry, which en-

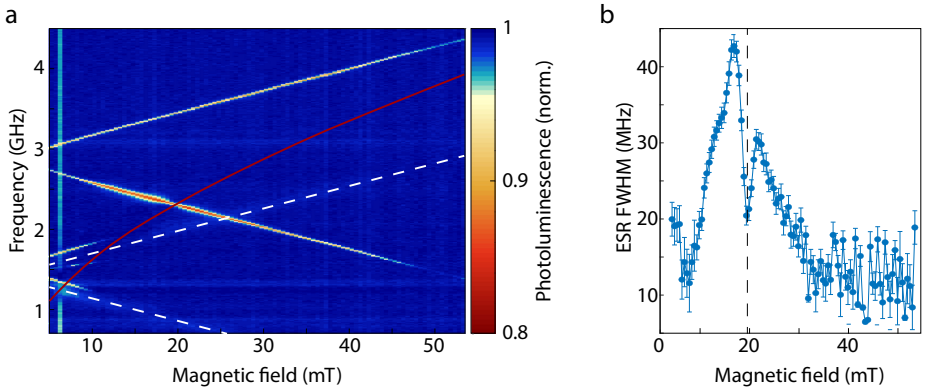

Figure 6.2: Electron spin resonance. (**a**) When an external microwave field is resonant with the NV ESR transitions, the NV spin is pumped into the dark $|\pm 1\rangle$ states, such that its luminescence is decreased. In the region close to where the ω_- transition crosses the calculated FMR of nickel (solid red line), the NV transition is additionally driven by the field of resonant spin waves. The dashed white lines indicate the frequency of ESR transitions in the NV excited states. (**b**) The full-width half-maximum (FWHM) of the ω_- transition is greatly enhanced close to the FMR of nickel, at a nickel-NV distance of 40±10 nm. Exactly at resonance (black dashed line), however, a sharp decrease is present.

6

tails preparing the NV spin in an eigenstate ($|0\rangle$, $|\pm 1\rangle$) and monitoring its time-relaxation caused by magnetic noise (Section 2.2.5). The spectrum of the magnetic noise can be probed by tuning the ESR transitions via the static field.

Close to the nickel film, the NV lifetime is reduced to few microseconds as a result of large transverse magnetic fluctuations at the NV ESR transitions (Fig. 6.3a-c). In the region of the diamond without nickel, the spin lifetime of NV centers is a few milliseconds (Fig. 6.3d), as expected[18–21] .

The spin-wave induced relaxation rates depends on several parameters, such as the NV-magnet distance, the spin-wavelength, the angle between the NV axis and the magnetization, the spin-wave propagation direction with respect to the magnetization, and the NV transition (Section 3.4, 3.5.2). As the distance is increased, the spin-wave stray field decays exponentially with distance, with a characteristic decay length similar to the spin-wavelength (Eq. 3.71-3.73). The spin-wave angle with respect with the magnetization, and the angle between the NV axis and the magnetization, influence the handedness and ellipticity of the spin-wave stray field at the NV location (Section 3.4). Finally, each NV transition is driven by a circularly polarized magnetic field, in the plane perpendicular to the NV axis, of opposite handedness (Section 2.2.4). Based on these considerations, we can draw some qualitative conclusions which are reflected in the measurements of Figure 6.3:

- The $|0\rangle \leftrightarrow |+1\rangle$ transition is not efficiently driven by spin-wave fields (Section 3.4-

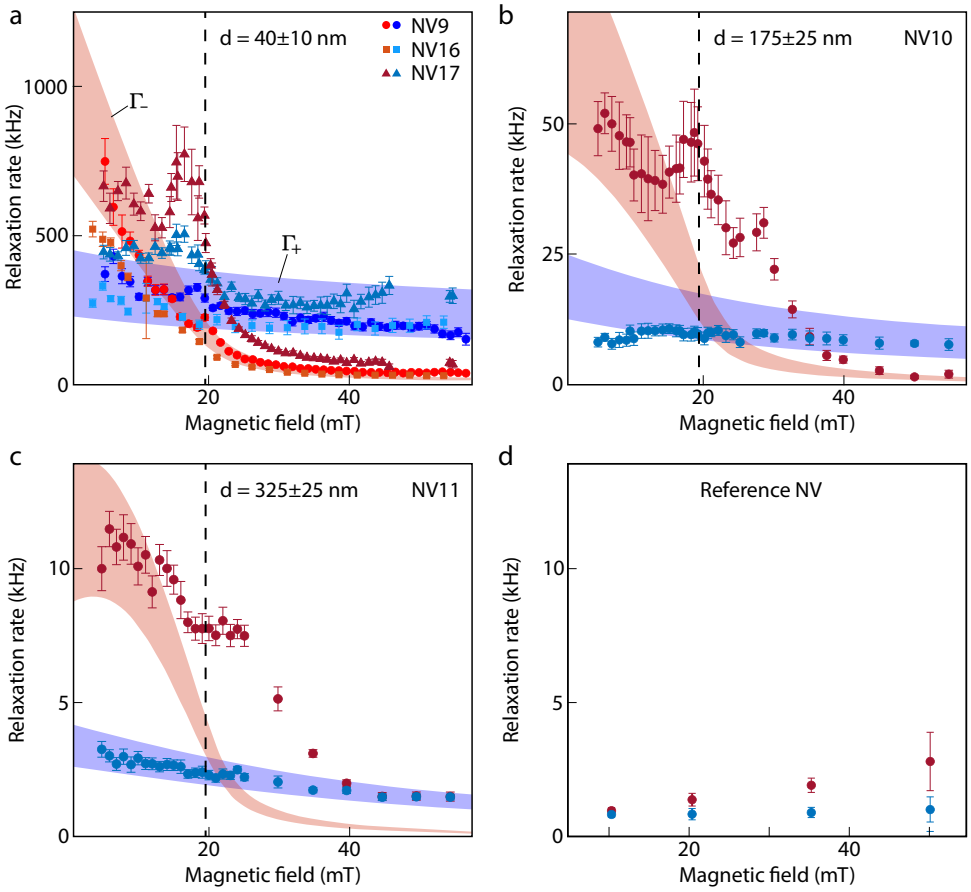

Figure 6.3: Probing the spin-wave spectrum via relaxometry. (**a**)-(**c**) Relaxation rate of NV centers at 40 ± 10, 175 ± 25 and 325 ± 25 nm from a nickel film, respectively. Red (blue) circles: Γ_- (Γ_+). The shaded red (blue) band is a calculations of Γ_- (Γ_+) based on the model of Chapter 3, taking into consideration the uncertainty on the NV-nickel distance. (**d**) The lifetime of shallow NV centers in bare diamond is typically between 0.5 and 5 ms (the latter being the coherence time in non-isotopically-purified bulk diamond at room temperature[18]). Red (blue) circles: Γ_- (Γ_+).

3.5.2). Additionally, its frequency runs almost parallel to the FMR (in Fig. 6.2a), such that spin waves of similar wavelength are probed at each field. Therefore, the relaxation rates Γ_+ is small, and almost constant with field.

- Conversely, the $|0\rangle \leftrightarrow |-1\rangle$ transition is efficiently driven by the spin-wave field. Above the FMR, this transition probes spin waves of different wavelength (longer wavelength towards the FMR), depending on the static field. At ~ 20 mT, ω_- crosses the FMR, such that at larger fields ω_- is not resonant with any spin-wave mode. Thus, Γ_- is large at small fields, and becomes much smaller than Γ_+ at large fields.

All these considerations are captured in the model introduced in Section 3.5.2, which is used to calculate the expected rates showed in figure 6.3 as shaded bands (which reflect the uncertainty on the NV-nickel distance). We find a generally good match between the model and the measurement. However, at the field where ω_- crosses the FMR of nickel (~ 20 mT), we observe discrepancies of unclear origin. Specifically, we detect relaxation rates for ω_- that, close to the FMR, exceeds the predicted ones by a factor 2-4, and that are dependent on which specific NV center is addressed.

It has been predicted that, below the FMR (i.e. in the spin-wave gap), two-magnon scattering events become important[3], while they are not captured by our theoretical model. Thus, this is a possible source of noise for fields larger than ~ 20 mT (i.e. below the FMR), but it does not justify the NV-specific variations. These variations could be partly explained by spatial inhomogeneities of the field, which we probe with additional measurements of NV Rabi frequencies (Section 6.5). An explanation of the possible mechanism responsible for the location-dependent variation of relaxation rates and Rabi frequency is in Section 6.5, corroborated by measurements of the film morphology (Section 6.4).

6.3. DISCUSSION

Using single NV sensor spins, we have probed the fluctuating magnetic fields generated by thermal spin waves in a nickel thin film. Our results are well-explained by the theory of chiral coupling between spin-wave fields and NV spins presented in Chapter 3. We find unexpected NV-specific variations of the Γ_- relaxation rate close to the FMR of nickel, which we investigate further by measuring NV Rabi frequencies, and that can be partially explained by local variations of the static field.

6.4. METHODS

The SiO_2 layer is grown by plasma-enhanced chemical vapor deposition (PECVD) at room temperature. The ramp is fabricated by shadowing half of the diamond with a rigid mask (a glass coverslide), suspended 1 µm above the diamond, similar to [1], during the SiO_2 growth. The ramp profile is measured with a profilometer (Fig. 6.4a). The resulting structure of the SiO_2 is granular, with grain size increasing with the layer thick-

ness (Fig. 6.4b-c). This is most likely due to the low temperature of the process, which was chosen in order to decrease the luminescence of the SiO_2 layer as much as possible, because films grown at high-temperature showed high luminescence that hampered the detection of single NV centers by drastically reducing the signal-to-noise ratio.

The nickel layer is evaporated on top of the diamond-SiO_2 substrate, masking half of the sample with tape to retain a nickel-free area of the diamond surface to use as location for reference measurements of NV relaxation rates.

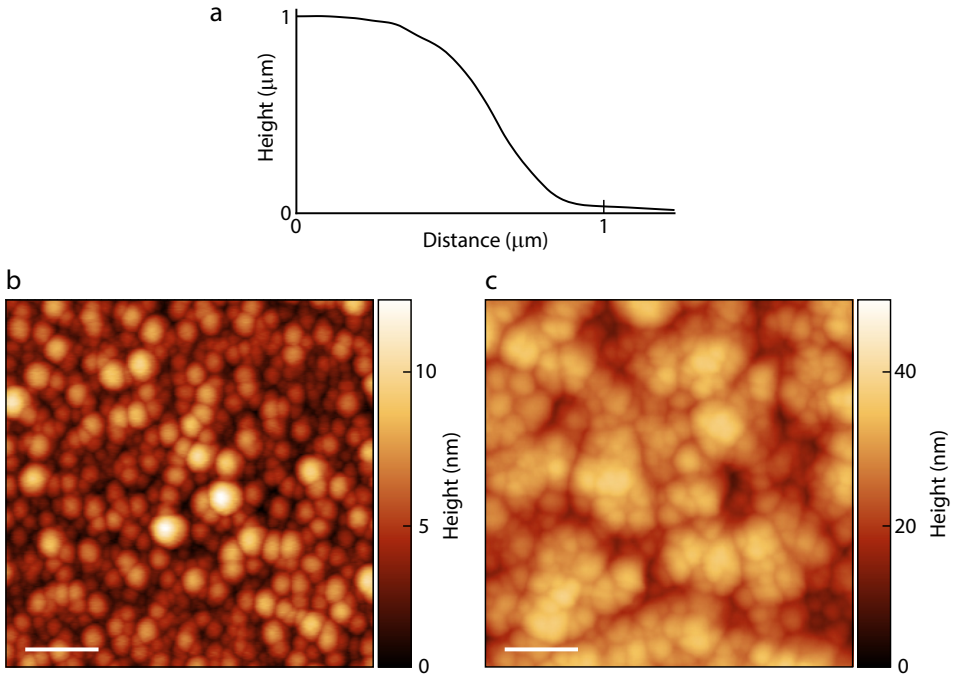

Figure 6.4: Ramp profile and structure. (**a**) Profilometry measurement of the SiO_2 spacer layer. (**b**)-(**c**) Atomic force microscope (AFM) measurement of the nickel film on a SiO_2 layer of thickness 50 nm and 1 μm, respectively. Scale bar, 100 nm.

6.5. ADDITIONAL MEASUREMENTS

PROBING COHERENT SPIN WAVES VIA RABI-FREQUENCY ENHANCEMENT

Because we find relevant discrepancies between the theoretically calculated and the experimentally measures relaxation rates, that seem to vary randomly with the specific NV center investigated, we perform additional measurements to uncover the reason of such local changes.

To probe the spin-wave driving of the NV spin, we perform Rabi oscillation measure-

ments (Section 2.2.4), which provide information regarding coherent spin waves. We first characterize the transmission through the microwave antenna used to excite spin waves by monitoring the Rabi frequency of an NV center in the bare diamond (Fig. 6.5a), which we use to normalize the measurements that follow, thereby making sure that the changes detected are caused by the magnetic film. While NV centers very close (30-50 nm) to the nickel present a large (~ 5-fold) change of the Rabi frequency (Fig. 6.5b), NVs that are hundreds of nanometers away show smaller (i.e. close to 20%) changes (Fig. 6.5c-d).

These results qualitatively remind of the Fano lineshape previously observed for NV centers interacting with a magnetic disk[16]. In the cited work, the variations were consistent with the NV location relative to the magnetic disk: the interference of the direct driving field and of that of the magnetic disk is position-dependent. In the present experiments we study a (supposedly) homogeneous film, which should induce no such variations. Thus, we deduce that the nickel film is, in fact, quite strongly not homogeneous, which is corroborated by the atomic force microscope measurements of Section 6.4. Assuming a granularity of the film allows to expect the presence of magnetic domains of diverse size and orientation, such that a situation similar to that of Ref. [16] is realized: the microwave driving field has a projection on the plane perpendicular to the magnetization that is position-dependent, and therefore a different driving efficiency (Section 3.2.1) in each domain, such that the amplitude of the spin-wave precession changes locally. Thus, the spin-wave field interferes with the direct field differently for each NV center, which can cause changes both in the amplitude and sign of the Fano lineshape[16].

It is reasonable to think that in our system there is an additional effect that stems from the domain structure[1]: the projection of the *static* magnetic field along the equilibrium magnetization of each domain is different. Thus, each magnetic domain possesses a distinct FMR frequency (according to Eq.3.42). This accounts for the frequency-shift of the center of the Fano-like resonances in Fig. 6.5.

INVESTIGATING THE LOCAL STRAY FIELD VARIATIONS

To corroborate the interpretation that the different response of each NV centers to spin-wave fields is caused by local inhomogeneities, we quantify the spatial variations of the stray magnetic field of the nickel film. To do so, we detect the local static field at the location of several neighbouring NV centers with the same orientation (Fig. 6.6), such that the field they experience should be equal[2]. In the space of just few micrometers, we find variations larger than 3 mT at an applied field of 20.5 mT. This confirms our assumptions regarding the possible presence of magnetic domains and inhomogeneities.

[1] If we assume that the structure of the nickel film is polycristalline, the non-negligible crystalline anisotropy of nickel results in each domain having the equilibrium magnetization oriented along different directions.

[2] A small field gradient is present, due to the finite size of the bar magnet used to apply the static field. Over an area of ~ 6 μm, such variations are in the tens of μT range.

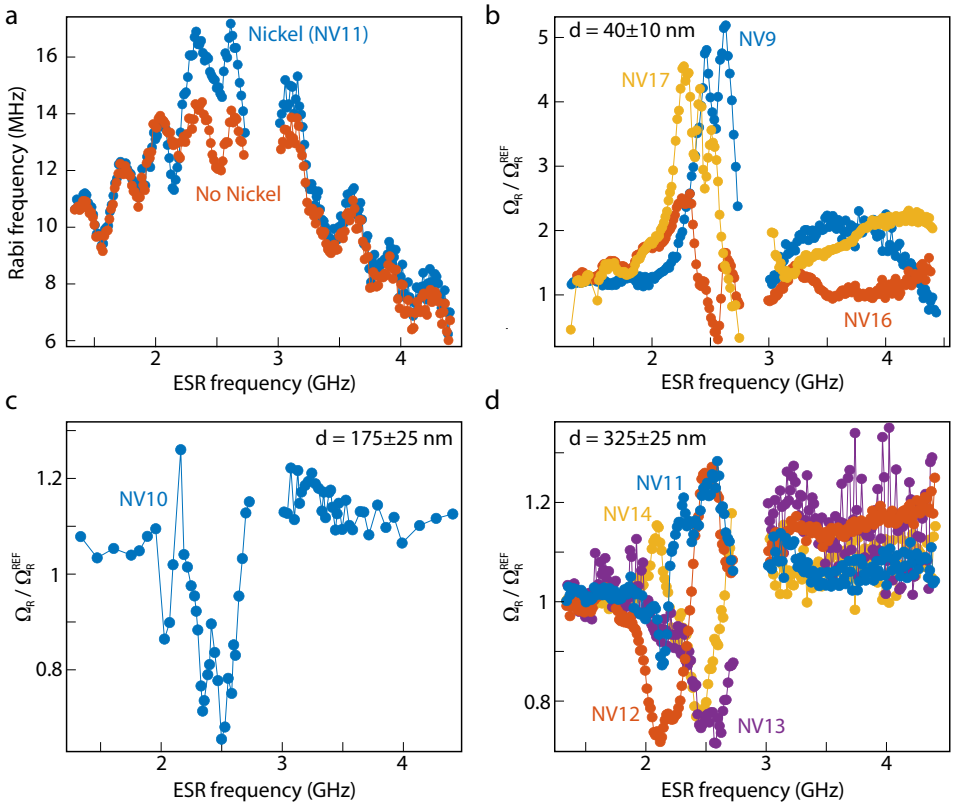

Figure 6.5: Detection of coherent spin-wave fields. (**a**) We calibrate the frequency-dependent delivery of microwaves through the electronics by characterizing the Rabi frequency of an NV center located in the bare diamond. An NV under the nickel shows a similar microwave transmission spectrum, on top of which are visible changes due to the magnetic film. Close to 2.87 GHz (the zero-field splitting of the NV center), the two ESR lines overlap, hindering a clean measurement of Rabi oscillations. (**b**) NV centers at 40 ± 10 nm from the nickel film show large changes of the Rabi frequency, between a ~5-fold enhancement and a reduction to almost zero. (**c**)-(**d**) At larger NV-Ni distances (175±25 and 325±25 nm, respectively), the spin-wave-induced changes are smaller. The variations of such changes, peculiar to each NV center, are discussed in the text.

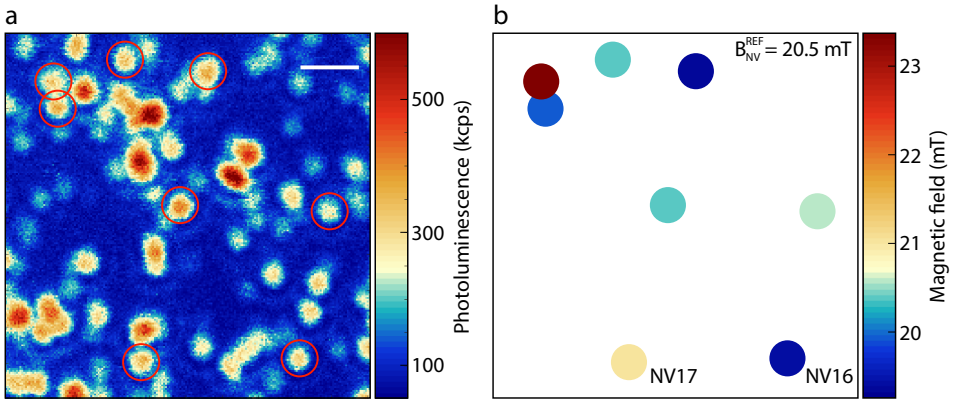

Figure 6.6: Local variations of the static stray field. (**a**) Photoluminescence image showing several NV centers close to each other. The circled NV centers have the same orientation of the NV axis, such that the stray field they experience should be the same. Scale bar: 1 µm . (**b**) For an applied static field of ~ 20.5 mT, the local field shows variations as large as 3 mT for NVs that are closer than 1 µm (top left corner).

6

REFERENCES

[1] S. Kolkowitz, A. Safira, A. A. High, R. C. Devlin, S. Choi, Q. P. Unterreithmeier, D. Patterson, A. S. Zibrov, V. E. Manucharyan, H. Park, and M. D. Lukin, *Probing Johnson noise and ballistic transport in normal metals with a single-spin qubit,* Science **347**, 1129 (2015).

[2] K. Agarwal, R. Schmidt, B. I. Halperin, V. Oganesyan, G. Zaránd, M. D. Lukin, and E. Demler, *Magnetic noise spectroscopy as a probe of local electronic correlations in two-dimensional systems,* Physical Review B **95**, 155107 (2017).

[3] B. Flebus and Y. Tserkovnyak, *Quantum-Impurity Relaxometry of Magnetization Dynamics,* Physical Review Letters **121**, 187204 (2018).

[4] S. Chatterjee, J. F. Rodriguez-Nieva, and E. Demler, *Diagnosing phases of magnetic insulators via noise magnetometry with spin qubits,* Physical Review B **99**, 104425 (2019).

[5] J. Cardellino, N. Scozzaro, M. Herman, A. J. Berger, C. Zhang, K. C. Fong, C. Jayaprakash, D. V. Pelekhov, and P. C. Hammel, *The effect of spin transport on spin lifetime in nanoscale systems,* Nature Nanotechnology **9**, 343 (2014).

[6] P. E. Dolgirev, S. Chatterjee, I. Esterlis, A. A. Zibrov, M. D. Lukin, N. Y. Yao, and E. Demler, *Characterizing two-dimensional superconductivity via nanoscale noise magnetometry with single-spin qubits,* (2021), arXiv:2106.05283v1 .

[7] N. J. McLaughlin, H. Wang, M. Huang, E. Lee-Wong, L. Hu, H. Lu, G. Q. Yan, G. D.

Gu, C. Wu, Y.-Z. You, and C. R. Du, *Observation of Superconductivity Induced Ferromagnetism in an Fe-Chalcogenide Superconductor,* (2021), arXiv:2106.15882 .

[8] G. Nava Antonio, I. Bertelli, B. G. Simon, R. Medapalli, D. Afanasiev, and T. van der Sar, *Magnetic imaging and statistical analysis of the metamagnetic phase transition of FeRh with electron spins in diamond,* Journal of Applied Physics **129**, 223904 (2021).

[9] B. Flebus, *Chemical potential of an antiferromagnetic magnon gas,* Physical Review B **100**, 064410 (2019).

[10] B. Flebus, H. Ochoa, P. Upadhyaya, and Y. Tserkovnyak, *Proposal for dynamic imaging of antiferromagnetic domain wall via quantum-impurity relaxometry,* Physical Review B **98**, 180409 (2018).

[11] T. I. Andersen, B. L. Dwyer, J. D. Sanchez-Yamagishi, J. F. Rodriguez-Nieva, K. Agarwal, K. Watanabe, T. Taniguchi, E. A. Demler, P. Kim, H. Park, and M. D. Lukin, *Electron-phonon instability in graphene revealed by global and local noise probes,* Science **364**, 154 (2019).

[12] F. K. K. Kirschner, F. Flicker, A. Yacoby, N. Y. Yao, and S. J. Blundell, *Proposal for the detection of magnetic monopoles in spin ice via nanoscale magnetometry,* Physical Review B **97**, 140402 (2018).

[13] J. F. Rodriguez-Nieva, K. Agarwal, T. Giamarchi, B. I. Halperin, M. D. Lukin, and E. Demler, *Probing one-dimensional systems via noise magnetometry with single spin qubits,* Physical Review B **98**, 195433 (2018).

[14] J. F. Rodriguez-Nieva, D. Podolsky, and E. Demler, *Hydrodynamic sound modes and Galilean symmetry breaking in a magnon fluid,* (2020), arXiv:1810.12333 .

[15] C. Du, T. van der Sar, T. X. Zhou, P. Upadhyaya, F. Casola, H. Zhang, M. C. Onbasli, C. A. Ross, R. L. Walsworth, Y. Tserkovnyak, and A. Yacoby, *Control and local measurement of the spin chemical potential in a magnetic insulator,* Science **357**, 195 (2017).

[16] T. van der Sar, F. Casola, R. Walsworth, and A. Yacoby, *Nanometre-scale probing of spin waves using single-electron spins,* Nature Communications **6**, 7886 (2015).

[17] F. Casola, T. van der Sar, and A. Yacoby, *Probing condensed matter physics with magnetometry based on nitrogen-vacancy centres in diamond,* Nature Reviews Materials **3**, 17088 (2018).

[18] A. Jarmola, A. Berzins, J. Smits, K. Smits, J. Prikulis, F. Gahbauer, R. Ferber, D. Erts, M. Auzinsh, and D. Budker, *Longitudinal spin-relaxation in nitrogen-vacancy centers in electron irradiated diamond,* Applied Physics Letters **107**, 242403 (2015).

[19] T. De Guillebon, B. Vindolet, J.-F. Roch, V. Jacques, and L. Rondin, *Temperature dependence of the longitudinal spin relaxation time T_1 of single nitrogen-vacancy centers in nanodiamonds,* Physical Review B **102**, 165427 (2020).

[20] M. Rollo, A. Finco, R. Tanos, F. Fabre, T. Devolder, I. Robert-Philip, and V. Jacques, *Quantitative study of the response of a single NV defect in diamond to magnetic noise,* Physical Review B **103**, 235418 (2021).

[21] A. Finco, A. Haykal, R. Tanos, F. Fabre, S. Chouaieb, W. Akhtar, I. Robert-Philip, W. Legrand, F. Ajejas, K. Bouzehouane, N. Reyren, T. Devolder, J.-P. Adam, J.-V. Kim, V. Cros, and V. Jacques, *Imaging non-collinear antiferromagnetic textures via single spin relaxometry,* Nature Communications 2021 12:1 **12**, 767 (2021).

[22] C. M. Purser, V. P. Bhallamudi, F. Guo, M. R. Page, Q. Guo, G. D. Fuchs, and P. C. Hammel, *Spinwave detection by nitrogen-vacancy centers in diamond as a function of probe-sample separation,* Applied Physics Letters **116**, 202401 (2020).

[23] B. A. McCullian, A. M. Thabt, B. A. Gray, A. L. Melendez, M. S. Wolf, V. L. Safonov, D. V. Pelekhov, V. P. Bhallamudi, M. R. Page, and P. C. Hammel, *Broadband multi-magnon relaxometry using a quantum spin sensor for high frequency ferromagnetic dynamics sensing,* Nature Communications **11**, 5229 (2020).